IEEE Access
Multidisciplinary | Rapid Review | Open Access Journal

Received February 22, 2019, accepted March 2, 2019, date of publication March 8, 2019, date of current version March 26, 2019.

*Digital Object Identifier 10.1109/ACCESS.2019.2903841*

# A Soft-Switching Control for Cascaded Buck-Boost Converters Without Zero-Crossing Detection

**JINGRONG YU, MAOYUN LIU, DONGRAN SONG, JIAN YANG, (Member, IEEE), AND MEI SU**
School of Automation, Central South University, Changsha 410083, China

Corresponding author: Dongran Song (humble_szy@163.com)

This work was supported in part by the Natural Science Foundation of Hunan Province of China under Grant 2017JJ2348, in part by the Research on Teaching Reform Project of Curriculum Design for Power Electronics Technology under Grant 2018jy062, and in part by the Fundamental Research Funds for the Central Universities of Central South University under Grant 2018zzts602.

**ABSTRACT** This paper proposes a novel soft-switching control without zero-crossing detection for the cascaded buck–boost converters (CBBCs). The proposed soft-switching control consists of two parts: soft-switching modulation and closed-loop control. In the modulation, the employed PWM approach is constructed by introducing a small negative current into the conventional PWM, and the soft-switching modulation based on the negative-current-based PWM is presented by adding a new switching process controlled by a modulation variable in the CBBC. In the closed-loop control, the relationship between the models of the negative-current-based PWM and the soft-switching modulation is deduced, and by utilizing the deduced relationship, the closed-loop control is designed while the PWM is modified to achieve the soft-switching. Meanwhile, to further reduce the ripple current and device losses, the parameter of the proposed control is optimized by refining the restrictive conditions. While the zero-crossing point of the inductor current is calculated with a given algorithm based on a current measurement, the circuit of zero-crossing detection is avoided. The validity and feasibility of the proposed soft-switching control approach are confirmed by the simulations and experiments on a 200-W prototype.

**INDEX TERMS** Soft-switching control, negative-current-based PWM, zero-crossing detection, optimal design, CBBC.

## I. INTRODUCTION

With the rapid depletion of fossil fuel reserves, the growing demand for electricity and the attention to climate change, a deep exploration in the field of renewable energy resource emerges. Buck or Boost converters are usually employed as the interface of storage unit in PV systems, fuel cell and electric vehicle, of which a major concern is that the change of environment affects the converter output voltage. For Buck or Boost converters, it is hard to satisfy the wide output voltage range and the bidirectional power flow [1], [2]. Therefore, in those applications, conventional Buck or Boost converters with a limited range of voltage regulation are unable to meet the requirements of engineering designs. The Cascaded Buck-Boost Converters (CBBC) shown in Figure 1, also called H-bridge buck-boost converter, is able to operate in both Buck and Boost modes while allowing the bidirectional energy flow, and thus suitable for the DC-DC transformation in the case of storage field [3]–[7]. For the control methods of the CBBC, the most common approach is the sectional

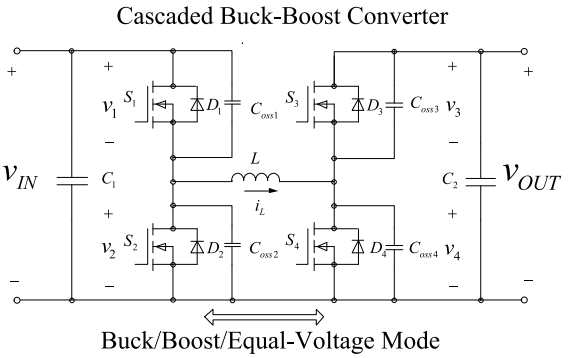


**FIGURE 1.** Schematic circuit diagram of a CBBC.

The associate editor coordinating the review of this manuscript and approving it for publication was Zhong Wu.

control [8]–[10], which operates the CBBC as the basic Buck converter, Boost converter or direct connection. However, the input and output voltages need to be compared in this approach, and the control modes need to be switched among different operation modes. To overcome the above shortcomings, PWM control is proposed, but it has an increasing switching loss due to the fact four switches are operated together [11], [12].

Nowadays, the issue of the increasing switching loss has drawn wide attentions, as the high switching frequency has been commonly applied that further increases the switching loss, especially in the situation of high voltage or large current [13], [14]. In order to reduce the switching loss, soft-switching approaches are widely applied to all kinds of power converters [15], [16]. In general, there are two ways to achieve soft-switching for DC-DC converters [17]: one way is to add the additional circuits to the main power circuit of the converter, while the other avoids the insertion of additional circuits and focuses on achieving soft-switching by operating the converter in discontinuous conduction mode (DCM).

In the way of adding additional circuits, some simple resonant circuits applied to the half-bridge CBBC have been presented in the literature [18]–[22]. The basic operating principle is to add the active and passive auxiliary components to resonate with the inductor or parasitic capacitors of the main circuit, and the switches of the converter can achieve soft-switching. Also various resonant circuits for CBBC are proposed in [23]–[26]. They ensure soft-switching of the switches in the main circuit, using a combination of active and passive auxiliary components. On the other hand, the resonant switching cell proposed in [27]–[29] provides the auxiliary resonant circuits formed by auxiliary switches, the active and passive components. However, these additional resonant circuits make the structure of the converters much more complicated, and bring about an uncertainty for the converters.

In order to avoid using additional circuits, the DCM-based soft-switching methods are presented. For the half-bridge CBBC, literature [15] proposes an approach. When the converter works in Buck mode or Boost mode, the top and the bottom switches act as main switches and auxiliary switches, respectively. This approach employs the original structure of the converter to form auxiliary switches instead of extra circuits, and switches the operation mode according to the values of input and output voltages. Literature [30] develops a half-bridge integrated zero-voltage-switching (ZVS) full-bridge converter, which features lower conduction loss and secondary-voltage stress. But the developed converter structure is sophisticated. A different approach achieving soft-switching for the bidirectional DC–DC converter is taken in [31]. The appropriate inductor is selected to make sure the direction of inductor current alternating in each switching cycle. The approach omits zero-crossing detection of the current, but it requires a high precision of inductance that is hardly guaranteed under different circumstances.

Aiming at a converter capable of realizing high efficiency and bidirectional power flow, a soft-switching modulation for CBBC is presented in [32]. The switches are gated in a way that the inductor current has a negative current at the beginning and the end of each pulse period, making the MOSFETs turn on when the antiparallel body diode is conducting. By solving the equations of inductor current, the switching time periods of the CBBC are calculated, and the open-loop control based on the switching time periods is developed. The patent [33] utilizes the same soft-switching method, and realizes the closed-loop control using analog circuits with a simple calculation. Literature [34] presents a control method with sectional phase-shift to achieve soft-switching. In this method, the modulation is adjusted according to the real-time input and output voltages, so the modulation is closely linked to control. The selection of phase shift directly affects the soft-switching and closed-loop control, and it is hard to decide the proper phase shift. And a digital control strategy with the same soft-switching strategy for CBBC is presented in [35]. Literature [36] proposed a constant frequency soft-switching control with minimum root mean square value of inductor current. The negative current is calculated and its value is about one third of the average current, while this relatively large negative current will influence the power transmission and system efficiency. A novel control concept for CBBC is presented in [37], while the PWM control signals are modulated depending on operating points to minimize the power losses. The optimal duty ratios are chosen in modulation, but a lot of restrictions in the selection process are needed.

The proposed control has been compared to the recent works mentioned above in the aspects of: the realization of closed-loop control, the utilization of zero-crossing detection, the value of $-I_0$ and the transmission efficiency. And the comparison is summarized in Table 1.

**TABLE 1. Comparison with recent works.**

| | Closed-Loop Control | Zero-Crossing Detection | Value of $-I_0$ | Efficiency |
|---|---|---|---|---|
| Soft-Switching in [32] | - | √ | Medium | 98.3% |
| Soft-Switching in [34] and [35] | √ | √ | Medium | 98.7% |
| Soft-Switching in [36] | √ | - | Large | 98.0% |
| Soft-Switching in [37] | √ | - | - | 97.79% |
| Patent [33] | √ | - | Large | 97% |
| Proposed Control | √ | - | Small | 98.8% |

When it is known that the closed-loop control has outstanding performance for disturbance restraint, the closed-loop control method is actually seldom studied for DCM-based CBBC. On one side, the CBBC has two legs, which means that there are two free variables in the control, thus the Single Input Single Output (SISO) control for CBBC should be

further studied. On the other side, the design goals of soft-switching modulation and closed-loop control are completely distinct, the traditional PWM control for CCM-based CBBC is unable not be applied directly. Hence, this study addresses these two difficulties and cooperates the soft-switching modulation with the closed-loop control, so it contributes the controls of CBBC.

In DCM, when the inductor current drops to zero, the inductor current flows backwards, which results in the current intrusion and a great fluctuation of the output voltage [38], [39]. To prevent the current intrusion phenomenon, the zero-crossing detection circuit is usually used in [32], [34], and [35], but it increases the system cost and its accuracy influences the control performance. In the proposed control, the zero-crossing detection circuit is avoided by introducing a current measurement at a specific point and the online calculation of the zero-crossing point of inductor current.

One of the advantages of the zero-crossing detection is that $-I_0$ can be controlled to increase the efficiency. By comparison, the method of timer and time calculation in [33], [36], and [37] would produce great error of $-I_0$, which will reduce the efficiency. To avoid the zero-crossing detection and improve efficiency, $-I_0$ is precisely controlled by calculation and an inductor current is measured to heighten the control accuracy.

Furthermore, literature [40] proposes an optimal control of the inductor current to achieve a high efficiency for all load conditions especially in light-load, but the way to reduce ripple value of inductor current for the soft-switching of CBBC operated in DCM has been rarely discussed in detail. In order to optimize the design of the soft-switching closed-loop control, the approaches of the ripple current reduction are presented as well.

Motivated by the afore-discussions, this study proposes a soft-switching closed-loop control for CBBC. With regards to the literatures, the major contribution of this study can be summarized as follows:

- The closed-loop control and modified PWM for soft-switching modulation are presented. The relationship of negative-current-based PWM ($-I_0$-based PWM) and the soft-switching modulation is deduced, and based on the deduced relationship, a modified PWM of the soft-switching can be realized in the same control structure for the soft-switching modulation. The design and the implementation of CBBC would be soundly simplified.
- A relatively large current is measured to maintain a higher calculation accuracy of $-I_0$, and the online zero-crossing calculation is introduced to replace the zero-crossing detection circuit.
- The optimization design for reducing the ripple current and the device loss is provided through optimal selection of the variables in the soft-switching closed-loop control.

The remainder of this paper is organized as follows. In Section II, the proposed soft-switching control strategy is provided, and the soft-switching modulation and closed-loop control are discussed in detail. Section III clarifies the optimal design of control parameter that would ensure soft-switching with a stable and better performance. Finally, Section IV presents the experimental results and discussion, while Section V concludes the paper.

## II. PROPOSED SOFT-SWITCHING CONTROL

The circuit of CBBC, as shown in Figure 1, is composed of four MOSFETs ($S_1$–$S_4$) with antiparallel body diodes ($D_1$–$D_4$) and parasitic capacitors ($C_{oss1}$–$C_{oss4}$), energy-storage inductor $L$, two filter capacitors $C_1$ together with $C_2$. Because of the symmetry of the converter structure, it can be achieved bidirectional power flow that features the same operation. In this paper, we choose a left-to-right power flow for research. The input voltage, the output voltage and the corresponding voltage on each switch are defined as $v_{IN}$, $v_{OUT}$ and $v_1$–$v_4$. For the CBBC circuit, the losses of MOSFETs have played a significant part in the total converter loss. In order to reduce the total loss and maintain a high efficiency of the CBBC, the soft-switching control is proposed.

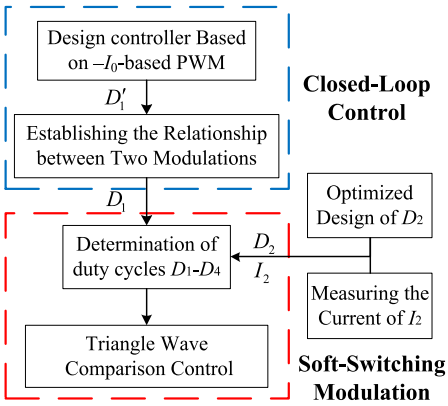


**FIGURE 2.** The overall framework of proposed soft-switching control for CBBC.

### A. FRAME OF THE SOFT-SWITCHING CONTROL

The overall framework of proposed soft-switching control for CBBC is shown in Figure 2, and it includes two parts: soft-switching modulation and closed-loop control.

The inductor current waveforms of proposed soft-switching control and $-I_0$-based PWM are shown in Figure 3(a) as $i_{L1}(t)$ and $i_{L2}(t)$, respectively.

The control process includes 4 steps:

1) The closed-loop control is established according to $-I_0$-based PWM to obtain the control variable as a duty cycle $D_1'$.

2) By comparing the model of $-I_0$-based PWM to the model of soft-switching modulation, $D_1'$ is converted into a duty cycle of soft-switching modulation as $D_1$.

3) An optimized $D_2$ and the measured inductor current $I_2$ at $t = (D_1 + D_2)T_S$ are utilized to calculate the duty cycles $D_1$–$D_4$ of soft-switching modulation.

4) The triangle wave comparison control is employed to get the control signals for each switch.

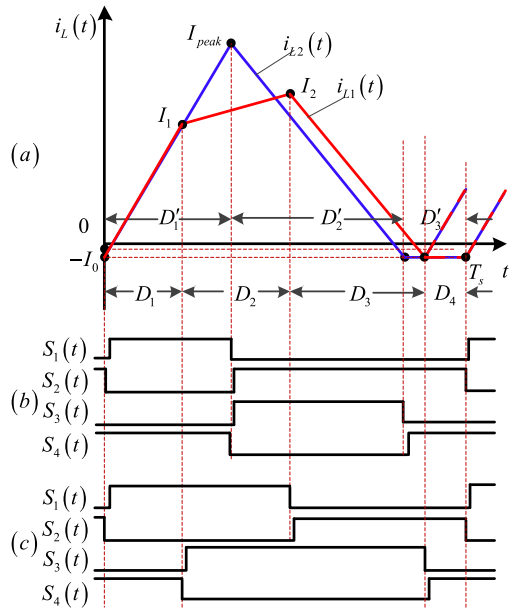


**FIGURE 3.** (a) Waveform diagram of inductor current for $-I_0$-Based PWM ($i_{L2}(t)$) and the soft-switching modulation ($i_{L1}(t)$) for Buck mode. (b) Control signals of $S_1$ to $S_4$ for $-I_0$-Based PWM. (c) Control signals of $S_1$ to $S_4$ for the soft-switching modulation.

In this proposed control, inductor current $I_2$ at $t = (D_1 + D_2)T_S$ is much larger than zero, which means the measurement of $I_2$ will have higher accuracy than the detection of zero-crossing point. Thus, by measuring $I_2$ and some simple calculation, the zero-crossing point of inductor current can be attained to avoid the zero-crossing detection circuit. Further the ripple current and the device loss are reduced by optimally designing the control parameter $D_2$.

### B. SOFT-SWITCHING MODULATION

For the CBBC with conventional PWM, the MOSFETs are divided into two groups: one group uses $S_1$ and $S_4$, and the other one uses $S_2$ and $S_3$, and the two groups are complementary in each switching cycle $T_S$ [17]. It is unnecessary to compare the input and output voltages, and the same control and modulation can be used in Buck mode, Boost mode and equal-voltage mode (where the input and output voltages are equal).

However, when the CBBC operates in DCM, the continuously increasing negative current ($-I_0$) will bring about the current intrusion. To avoid the current intrusion, $-I_0$-based PWM based on the conventional PWM is proposed in this paper, which creates a continuous current circuit when the inductor current is negative. By doing that, the inductor current continues to be $-I_0$ until the end of this switching cycle, and the $-I_0$ is employed to design the specific switching sequence of soft-switching.

The inductor current waveform of $-I_0$-based PWM is shown in Figure 3(a) for CBBC in Buck mode, and the control signals of each switch are shown in Figure 3(b).

*Stage 1* ($0 < t \le D_1'T_S$): The switches $S_1$ and $S_4$ are turned on while $S_2$ and $S_3$ are turned off. In this period, the input voltage passes through the inductor to store energy, which leads to the increase of the inductor current.

*Stage 2* ($D_1'T_S < t \le (D_1' + D_2')T_S$): The switches $S_1$ and $S_4$ are turned off while $S_2$ and $S_3$ are turned on. At that time, the electric energy stored by the inductor is transferred to the output, so the inductor current is reduced to the negative.

*Stage 3* ($(D_1' + D_2')T_S < t \le T_S$): When the inductor current reaches $-I_0$ that is closed to 0 at $t = (D_1' + D_2')T_S$, turning off $S_3$ and turning on $S_4$ create a new switching process for the soft-switching modulation. In the last time period $(D_1' + D_2')T_S < t \le T_S$, the switches keep unchanged, while the inductor does not transmit energy at that time. Due to the freewheeling process, the inductor current remains $-I_0$. In addition, there is a commonly used dead time in the control signals of each switch.

In light of the charging and discharging processes of inductor and capacitor mentioned above, the differential equations that represent the dynamical behaviors of the circuit are given by

$$C_2\frac{dv_{OUT}}{dt} = \begin{cases} -v_{OUT}/R & 0 \le t < D_1'T_S \\ i_L - v_{OUT}/R & D_1'T_S \le t < (D_1' + D_2')T_S \\ -v_{OUT}/R & (D_1' + D_2')T_S \le t < T_S \end{cases} \quad (1)$$

$$L\frac{di_L}{dt} = \begin{cases} v_{IN} & 0 \le t < D_1'T_S \\ -v_{OUT} & D_1'T_S \le t < (D_1' + D_2')_2 T_S \\ 0 & (D_1' + D_2')T_S \le t < T_S \end{cases} \quad (2)$$

where $i_L$ is defined as the inductor current.

As shown in Figure 3(a), $I_{peak}$ is the steady-state peak value of inductor current, while $k_1$ and $k_2$ are the rising and falling slopes of inductor current in $i_{L2}(t)$, respectively. According to geometric relationship of inductor current in the steady state, $k_1$, $k_2$ and $I_{peak}$ are calculated by:

$$k_1 = \frac{V_{IN}}{L} \quad (3)$$

$$k_2 = -\frac{V_{OUT}}{L} \quad (4)$$

$$I_{peak} = \frac{V_{IN}}{L}D_1'T_S - I_0 = \frac{V_{OUT}}{L}D_2'T_S - I_0 \quad (5)$$

where $V_{IN}$, $V_{OUT}$, $R$, $D_1'$ and $D_2'$ are steady-state input voltage, output voltage, output resistor, charging duty ratio and discharging duty ratio, respectively. It is noteworthy that $-I_0$ is not the minimum inductor current due to the function of inductance discharging.

Solving (5), it gets the relation between $D_1'$ and $D_2'$:

$$D_2' = \frac{V_{IN}}{V_{OUT}}D_1' \quad (6)$$

The steady-state mean value of the current flowing through the capacitor $C_2$ is denoted $\bar{I}_{C2,1}$ , and it is calculated on the basis of the waveform of $i_{L2}(t)$ as:

$$\begin{aligned} \bar{I}_{C2,1} &= \frac{I_{peak} + I_0}{2}D_2' - D_2'I_0 - \frac{V_{OUT}}{R} \\ &\approx \frac{V_{IN}}{2L}D_1'D_2'T_S - \frac{V_{OUT}}{R} \end{aligned} \quad (7)$$

where the inductor current determining the voltage control through (1) could be obtained by the area of the specific current. During the period between $D_1'T_S$ and $(D_1' + D_2')T_S$, $-I_0$ is much smaller than the rest of the switching cycle, so it can be ignored. Substituting (6) into (7) yields:

$$\bar{I}_{C2,1} = \frac{V_{IN}^2}{2LV_{OUT}} D_1^2 T_S - \frac{V_{OUT}}{R} \tag{8}$$

The capacitor current in (8) is equivalent to the inductor current in (1), and the $-I_0$-based PWM can be designed according to (1).

The approach of $-I_0$-based PWM has the advantage of simple realization and safe operation especially in equal-voltage mode, but it has the drawback of increasing switching loss. In order to improve the efficiency of CBBC, the soft-switching modulation approach is presented based on the principle: the antiparallel body diode of the MOSFET should be on before turning on the MOSFET, while parasitic capacitor should be charged firstly when the switch is turned off. In order to do that, a new set of switch states is added to $-I_0$-based PWM, so four switches are conducted in the order of $S_1$-$S_3$-$S_2$-$S_4$. The mechanism for achieving soft-switching of all switches can be fully explained in accordance with the equivalent circuits shown in Figure 4.

In each switching cycle, there are ten different switching processes, and each equivalent circuit in Figure 4 represents one switch state.

*Stage 1* ($0 < t < D_1T_S$ and $i_L < 0$): When the time starts at zero, the energy stored by the inductor $L$ flows into the input side through the antiparallel body diodes of $S_1$ and $S_4$. After the dead time for $S_1$ and $S_2$, $S_1$ is turned on at soft-switching state, as shown in Figure 4(a).

*Stage 2* ($0 < t < D_1T_S$ and $i_L > 0$): As the energy in $L$ dissipated, the input voltage $v_{IN}$ charges $L$, while $C_{oss1}$ and $C_{oss4}$ are completely discharged through $S_1$ and $S_4$, in Figure 4(b).

*Stage 3* ($t = D_1T_S$): At this point, $i_L$ charges $C_{oss4}$ while $S_4$ is turned off simultaneously to reduce the switching losses of $S_4$, as shown in Figure 4(c).

*Stage 4* ($D_1T_S < t < (D_1 + D_2)T_S$): At the end of the dead time for $S_3$ and $S_4$, the full charge of $C_{oss4}$ is accomplished, and the antiparallel body diode of $S_3$ takes over the current. Where, the charging-discharging status of the inductor $L$ depends on the difference of input and output voltage, so that $S_3$ is naturally turned on at soft-switching state, as depicted by Figure 4(d).

*Stage 5* ($t = (D_1 + D_2)T_S$): $i_L$ charges $C_{oss1}$ while $S_1$ is turned off at the same time to achieve low switching losses of $S_1$, as depicted by Figure 4(e).

*Stage 6* ($(D_1 + D_2)T_S < t < (D_1 + D_2 + D_3)T_S = (1 - D_4)T_S$ and $i_L > 0$): In the period of dead time for $S_1$ and $S_2$, the full charge of $C_{oss1}$ is accomplished, and the current flows through the antiparallel body diode of $S_2$. Where, $L$ discharges to the output voltage $v$ so that $S_2$is turned on at soft-switching state, as depicted by Figure 4(f).

*Stage 7* ($(D_1 + D_2)T_S < t < (1 - D_4)T_S$ and $i_L < 0$): When $i_L$ changes direction, the output voltage $v_{OUT}$ charges $L$ while $C_{oss2}$ and $C_{oss3}$ are completely discharged through $S_2$ and $S_3$ as shown in Figure 4(g).

*Stage 8* ($t = (1-D_4)T_S$): As $S_2$ and $S_3$ remain conductive, $i_L$ steadily drops until it reaches $-I_0$ when $t = (1 - D_4)T_S$, and then $S_3$ is turned off as shown in Figure 4(h). Due to the freewheeling of the inductor current, the value of inductor current will decrease to a negative value more than $-I_0$ in this time period. The light value of inductance makes the minimum inductor current just slightly smaller than $-I_0$, so the minimum inductor current is regarded as $-I_0$.

*Stage 9* ($(1–D_4)T_S < t < T_S$): At the end of the dead time for $S_3$ and $S_4$, the charge of $C_{oss3}$ is accomplished, the antiparallel body diode of $S_4$ takes over the current, and $S_4$ is turned on after dead time to achieve soft-switching of $S_3$ and $S_4$. In the process, $i_L$ keeps unchanged until the next switch period, as shown in Figure 4(i).

*Stage 10* ($t = T_S$): Similarly, $S_2$ is turned off in a low-loss state in Figure 4(j)

In general, such switching sequence generates relatively low losses especially when the converter operates under high switching frequency or high voltage.

### C. CLOSED-LOOP CONTROL

The arithmetical relation between the models of $-I_0$-based PWM and soft-switching modulation is essential for the soft-switching control. Therefore, the model of soft-switching modulation is firstly built as follows.

The inductor current waveforms $i_{L1}(t)$ of CBBC with the soft-switching modulation in Buck mode is depicted in Figure 3(a). Based on the charging and discharging processes of inductor and capacitor for the soft-switching modulation discussed above, the dynamical behaviors of capacitor and inductor are formulated as

$$C_2 \frac{dv_{OUT}}{dt} = \begin{cases} -v_{OUT}/R & 0 \le t < D_1T_S \\ i_L - v_{OUT}/R & D_1T_S \le t < (D_1 + D_2)\,T_S \\ i_L - v_{OUT}/R & (D_1 + D_2)\,T_S \le t < (1 - D_4)\,T_S \\ -v_{OUT}/R & (1 - D_4)\,T_S \le t < T_S \end{cases} \tag{9}$$

$$L \frac{di_L}{dt} = \begin{cases} v_{IN} & 0 \le t < D_1T_S \\ v_{IN} - v_{OUT} & D_1T_S \le t < (D_1 + D_2)\,T_S \\ -v_{OUT} & (D_1 + D_2)\,T_S \le t < (1 - D_4)\,T_S \\ 0 & (1 - D_4)\,T_S \le t < T_S \end{cases} \tag{10}$$

In the steady state, the internal relations among $I_1$, $I_2$ and duty cycles can be obtained according to Figure 3 as:

$$\begin{cases} I_1 = \frac{V_{IN}}{L} D_1T_S - I_0 \\ I_2 - I_1 = \frac{V_{IN} - V_{OUT}}{L} D_2T_S \\ I_2 = \frac{V_{OUT}}{L} D_3T_S - I_0 \\ D_1 + D_2 + D_3 + D_4 = 1 \end{cases} \tag{11}$$

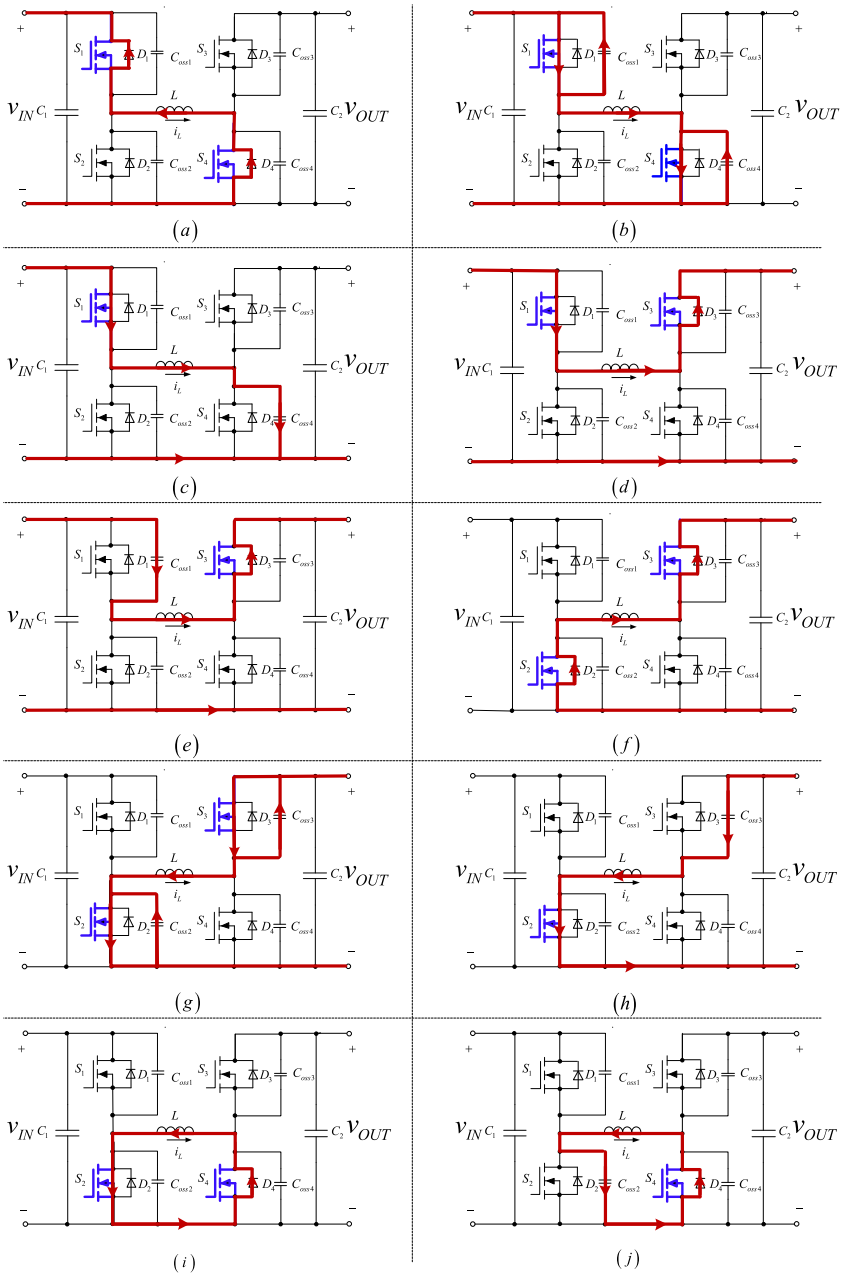


**FIGURE 4.** EquivalenT circuit diagrams for the soft-switching modulation of CBBC. (a) $0 < t < D_1T_S$ and $i_L < 0$. (b) $0 < t < D_1T_S$ and $i_L > 0$. (c) $t = D_1T_S$. (d) $D_1T_S < t < (D_1 + D_2)T_S$. (e) $t = (D_1 + D_2)T_S$. (f) $(D_1 + D_2)T_S < t < (D_1 + D_2 + D_3)T_S = (1 - D_4)T_S$ and $i_L > 0$. (g) $(D_1 + D_2)T_S < t < (1 - D_4)T_S$ and $i_L < 0$. (h) $t = (1 - D_4)T_S$. (i) $(1 - D_4)T_S < t < T_S$. (j) $t = T_S$.

The mean value of the current flowing through the capacitor $C_2$ called $\bar{I}_{C2,2}$ can be calculated by:

$$\bar{I}_{C2,2} = \frac{I_1 + I_2 + 2I_0}{2} D_2 + \frac{I_2 + I_0}{2} D_3 - (D_2 + D_3) I_0 - \frac{V_{OUT}}{R} \quad (12)$$

The mean value of the inductor current $\bar{I}_L$ is solved as:

$$\bar{I}_L = \frac{I_1 + I_0}{2} D_1 + \frac{I_1 + I_2 + 2I_0}{2} D_2 + \frac{I_2 + I_0}{2} D_3 - I_0 \quad (13)$$

To indicate the functional relationship among steady-state duty cycles $D_1$, $D_2$, $D_3$ and $D_4$, (11) is simplified as

$$D_3 = \begin{cases} \left(I_1 + \frac{V_{IN} - V_{OUT}}{L} D_2 T_S + I_0\right) \Big/ \frac{V_{OUT} T_S}{L} \\ (I_2 + I_0) \Big/ \frac{V_{OUT} T_S}{L} \end{cases} \quad (14)$$

From (14), $D_3$ can be calculated according to the measurement of inductor current $I_1$ or $I_2$.

Substituting (11) into (12) and neglecting $-I_0$ yields

$$\bar{I}_{C2,2} \approx \frac{T_S V_{IN}^2}{LV_{OUT}} D_1 D_2 + \frac{T_S \left(V_{IN}^2 - V_{OUT} V_{IN}\right)}{2LV_{OUT}} D_2^2 + \frac{T_S V_{IN}^2}{2LV_{OUT}} D_1^2 - \frac{V_{OUT}}{R} \quad (15)$$

Supposing that the average values of the current flowing through $C_2$ in (8) and (15) are equal, it yields

$$D_1 = \sqrt{\frac{V_{OUT} D_2^2 + V_{IN} D_1^2}{V_{IN}}} - D_2 \quad (16)$$

where the function of $D_1'$ is obtained from Proportion Integration (PI) controller with the $-I_0$-based PWM. Besides, $D_2$ is an uncertain variable that has some restrictions and influents on the performance of soft-switching, and will be discussed in next section.

With the principle of voltage-second balance, the inductor current integral in the time period $D_2' T_S$ is equal to that of $D_2 T_S + D_3 T_S$ as shown in Figure 3.

By employing (16), the PI control with $-I_0$-based PWM for controlling the output voltage can be used in CBBC with DCM-based soft-switching modulation.

Only the output voltage control loop exists because the mean value of inductor current is too small to be controlled individually in DCM. In the PI control, the output value of PI controller is the duty cycle $D_1'$, so the control approach ensures the desired output voltage even if the load changes. Since the system is nonlinear, the state average model of CBBC with $-I_0$-based PWM is used for designing the output voltage control loop. And considering the directivity of the variables, the state average model of different modes can be defined uniformly as

$$C_2 \frac{d\left\langle v_{OUT}(t)\right\rangle_{T_S}}{dt} = \frac{\left\langle v_{IN}(t)\right\rangle_{T_S}^2}{2L\left\langle v_{OUT}(t)\right\rangle_{T_S}} d_1^2(t) T_S - \frac{\left\langle v_{OUT}(t)\right\rangle_{T_S}}{R} \quad (17)$$

where $\langle v_{IN}(t)_{T_S}\rangle$ and $\langle v_{OUT}(t)_{T_S}\rangle$ are the state mean values of input and output voltages. Using (17), the steady state model applying Laplace transform is established by:

$$G_{vd}(s) = \frac{V_{IN}^2 D_1 R T_S}{LC_2 R V_{OUT} s + 2LV_{OUT}} \quad (18)$$

where $G_{\mathrm{vd}}(\mathrm{s})$ is the transfer function of $V_{\mathrm{OUT}}$ versus $D_1'$.

The parameters $K_{\mathrm{p}}$ and $K_{\mathrm{i}}$ of the PI controller are selected such that the voltage control loop is regarded as typical second-order systems in Buck mode, Boost mode and equal-voltage mode. In addition, the parameters of $G_{\mathrm{vd}}(\mathrm{s})$ differ in each operating condition, due to an alteration of capacitor of $C_2$ and different voltage transfer ratios. As a consequence, $K_{\mathrm{p}}$ and $K_{\mathrm{i}}$ have to be adapted to parameter variations.

### D. ZERO-CROSSING CALCULATION OF INDUCTOR CURRENT

With regard to the traditional soft-switching method with zero-crossing detection, it is difficult to guarantee the accurate detection of zero point. And the precision of the detection as well as the switching speed have significant impact on the soft-switching effect.

Instead of zero-crossing detection continuously, a current measurement at specific instant is carried out in the proposed soft-switching control, and a calculation of zero-crossing point is introduced to avoid the zero-crossing detection.

In the modeling of CBBC with soft-switching modulation, the negative inductor current $-I_0$ is considered into the model, thus in the proposed control, the time period $D_1$ for soft-switching modulation are calculated according to (16). The given value of $-I_0$ is a small value closed to zero, so it can be neglected in the calculation process of (16). A measurement of $I_1$ or $I_2$ is introduced when calculating $D_3$. At this point, with the known optimal variable of $D_2$, the calculated value of $D_1$ and the measured$I_1$ or $I_2$, $D_3$ are obtained according to (14). While $-I_0$ can be accurately controlled to a given value closed to zero through (19).

$$I_0 = \begin{cases} \frac{V_{OUT}}{L} D_3 T_S - \frac{V_{IN} - V_{OUT}}{L} D_2 T_S - I_1 \\ \frac{V_{OUT}}{L} D_3 T_S - I_2 \end{cases} \quad (19)$$

In the implementation of CBBC, the sampling inductor current at $D_1 T_S$ or $(D_1 + D_2)\, T_S$ as $I_1$ or $I_2$ is employed for system current protection, because$I_1$ or $I_2$ is the peak current in different modes as shown in Figure 5. Concretely, $I_2$ is the nearest turning point to $-I_0$ which simplifies the calculation process and time. While $I_1$ is measured at the steadiest stage of current change where the error caused by the delay of the measurement system is less affected. The large measuring values of $I_1$ and $I_2$ have higher detection accuracy and are conducive to zero-crossing point calculation comparing with the small current. Meanwhile, the measurement of inductor current is benefit to suppress the continuous increase of $-I_0$ and enlarge the transmission power as well as the efficiency of CBBC. In addition, choosing whether to measure $I_1$ or $I_2$ will be further compared in the experiment section.

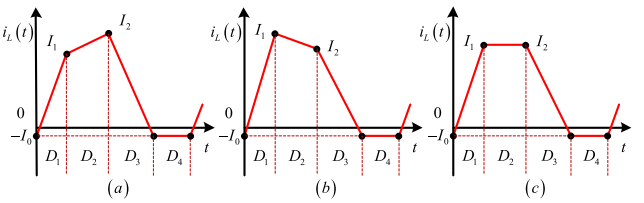


**FIGURE 5.** Waveform diagram of inductor current for proposed soft-switching control. (a) Buck mode. (b) Boost mode. (c) Equal-voltage mode.

*Remark 1:* In the case of the timing error, the output voltage under the closed-loop control is not influenced, while the soft-switching affected in the current switching cycle can be recalculated and corrected in the next switching cycle. Further some observer-based adaptive control methods can be employed in the case of the component parameters variation.

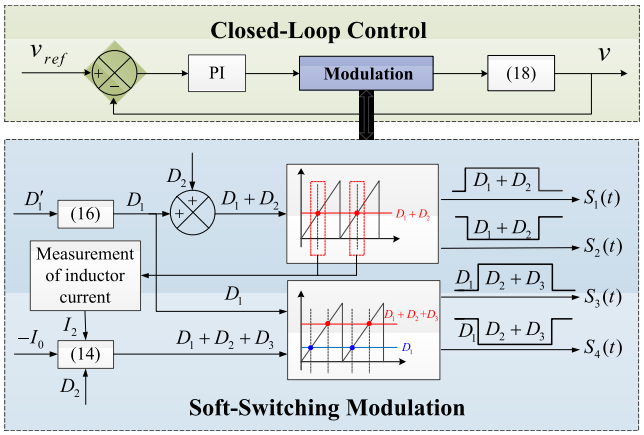


**FIGURE 6.** Proposed soft-switching control approach for CBBC.

### *E. IMPLEMENTATION OF THE PROPOSED SOFT-SWITCHING CONTROL*

As demonstrated in Figure 6, the control approach consists of closed-loop control and soft-switching modulation. The control algorithm is realized on the DSP TMS320C28335 chip.

In the process of implementation, PI control is designed to control the output voltage by software to obtain $D_1'$. The PWM waveform which is set to $D_1'$ is improved according to (16). In this way, initial $D_1$ for the soft-switching modulation will be achieved in every switching cycle. After that, the control signals of$S_1(t)$ and $S_2(t)$ are obtained by comparing the triangular wave with the duty cycle $D_1 + D_2$. Similarly, $S_3(t)$ and $S_4(t)$ operate in the light of the duty cycle $D_2 + D_3$ through the triangular wave comparison, and the rising edge is received at $D_1$ while the trailing edge is got at $D_1 + D_2 + D_3$. The duty cycle $D_3$ can be calculated based on (14) and $D_2$ is a given value that can be optimized. In (14), an interrupt has occurred to measure the value of $I_2$ when the control signal of $D_1 + D_2$ flips that is $t = (D_1 + D_2)T_S$, and $I_2$ is the value measured in the last switching cycle. While the measurement of $I_1$ can be attained in the same way. The dead time of the control signals for each switch is introduced to eliminate the effect of the turn-off delay and ensure the full charge of the parasitic capacitors simultaneously.

## III. OPTIMAL DESIGN OF CONTROL PARAMETERS

The selection of control parameters is critical to the achievement of the proposed soft-switching control for CBBC. Since there is a degree of freedom to optimize according to (11), the ripple current and device losses are chosen to be improved under steady state.

### *A. OPTIMIZED RIPPLE CURRENT*

The ripple current is the high harmonic component of the current. Due to the large change of the current amplitude, the current ripple may directly affect the performance of the switching power supply. Operating in the DCM mode, the CBBC can be designed with a low inductance, but its inductor current is relatively large.

The peak current can be expressed in (20) for Buck mode and (21) for Boost mode.

$$I_{peak} = D_3 \frac{V_{OUT} T_S}{L} - I_0 \tag{20}$$

$$I_{peak} = D_1 \frac{V_{IN} T_S}{L} - I_0 \tag{21}$$

By using (14), (16), (20) and (21), the inductor current ripple $\Delta I_L$ can be expressed as

$$\begin{aligned} \Delta I_L &= I_{peak} + I_0 \\ &= \begin{cases} \left( \sqrt{V_{OUT} V_{IN} D_2^2 + V_{IN}^2 D_1^2} - V_{OUT} D_2 \right) \frac{T_S}{L} \ (a) \\ \left( \sqrt{V_{OUT} V_{IN} D_2^2 + V_{IN}^2 D_1^2} - V_{IN} D_2 \right) \frac{T_S}{L} \ (b) \end{cases} \end{aligned} \tag{22}$$

where (22-a) is for Buck mode and (22-b) is for Boost mode. As $\Delta I_L$ alters for every operation mode, its value is used to satisfy the system requirements. When the system parameters and the input and output voltages are fixed, it is only related to the variable $D_2$.

### *B. OPTIMIZED DEVICE LOSSES*

Device losses contributes a large part of the total losses of a DC-DC converter, particularly for a high switching frequency. For the device losses of CBBC, they consist of switching losses and conduction loss, which can be expressed as:

$$P_{loss} = P_{con} + P_{sw} \tag{23}$$

where $P_{sw}$ is switching losses, and$P_{con}$ is defined as conduction loss,

The switching losses comprise the turn-on loss and turn-off loss of MOSFETs and its antiparallel body diode, and the losses of MOSFET's parasitic capacitors. For the CBBC, the turn-on loss and turn-off loss of the MOSFETs can be ignored because of the soft-switching modulation, while it is usually neglected for the antiparallel body diodes. Hence, the switching losses can be calculated as:

$$P_{sw} = 2C_{oss} V_{DS}^2 \tag{24}$$

where $V_{DS}$ is the voltage between the drain pole $D$ and the source $S$ at the cut-off time.

The conduction loss of CBBC could be evaluated by the loss estimation method in [41]:

$$\begin{aligned} P_{con} = {} & (2D_1 + D_2)^2 I_{RMS}^2 R_{ds(on)} + (1 - D_2 - 2D_1) V_{SD} I_{DS} \\ & + (D_2 + 2D_3) V_{SD} I_{RMS} + (1 - D_2 - 2D_3)^2 I_{DS}^2 R_{ds(on)} \end{aligned} \tag{25}$$

where, $I_{DS}$ is the leakage current at the actual junction temperature at the cut-off time, $V_{SD}$ is the forward voltage drop of the antiparallel body diode of the power MOSFET, $I_{RMS}$ is the effective current of the inductor, and the average inductor current can be expressed by the average inductor current in

the case of direct-current as (13). And $R_{ds(on)}$ is the resistance between $D$ and $S$ when it is conducted.

The device losses of the proposed soft-switching control can be calculated according to (13) (23), (24) and (25). And the formula of the device losses can be simplified on the basis of (11), (14) and (16) while neglecting $-I_0$. After that, the device losses can be expressed in terms of $D_2$.

### C. VARIABLE SELECTION

In the proposed soft-switching control, there is no sufficient condition to ensure each switching stage distinctly, so a given variable of duty cycle is added. Based on that, the ripple current and the device losses connect to $D_2$, so $D_2$ is chosen to be the variable to achieve the optimal design.

Before the selection of $D_2$, the duty cycles have a certain range of value, those are, $D_4 \geq 0$, $D_1$, $D_2$ and $D_3$ are more than zero at the same time to ensure the specific conduction sequence. After substituting (8) into (1), setting the left half of (1) to zero, $D_1'$ is got as (26). And substituting (26) into (11), (14) and (16) can obtain the range of $D_2$ as (27).

$$D_1^2 = \frac{2LV_{OUT}^2}{T_S R V_{IN}^2} \tag{26}$$

$$\begin{cases} D_1 = \sqrt{\left(V_{OUT}D_2^2 + V_{OUT}D_1^2\right)/V_{IN}} - D_2 > 0 \\ D_2 > 0 \\ D_3 = \sqrt{\left(V_{OUT}V_{IN}D_2^2 + V_{IN}^2D_1^2\right)/V_{OUT}^2} - D_2 > 0 \\ D_4 = 1 - D_1 - D_2 - D_3 \geq 0 \end{cases} \tag{27}$$

In order to achieve low ripple current and low device losses, $D_2$ is optimized according to (22) and (23). It is obvious that $D_2$ specified by (27) is better to keep it as large as necessary with a certain safety margin in case of abnormal condition when CBBC works in maximum power condition. As results, the obtained value of $D_2$ can not only achieve the soft-switching successfully but also lead to a higher system operation effect, which makes the ripple current and device losses smaller.

*Remark 2:* Since there is only control freedom to optimize the maximum power limit and medium/light load conduction loss, a tradeoff between the two has to be made.

## IV. EXPERIMENTAL RESULTS

The performance of the proposed soft-switching control approach is tested and evaluated on a 200W CBBC prototype. For the purpose of performance evaluation, this same converter is also tested with using $-I_0$-based PWM approach and sectional control. The overall framework and principle of experimental platform is depicted in Figure 7, and the actual platform is shown in Figure 8. The whole system consists of three parts: control circuit board, sampling board and switch devices board. The control system uses a DSP + CPLD structure with TMS320C28335 DSP and XC9572XL CPLD chips. The sampling system includes hall sensors (CHV-25P and CHB-25NP) and hardware protection circuits.

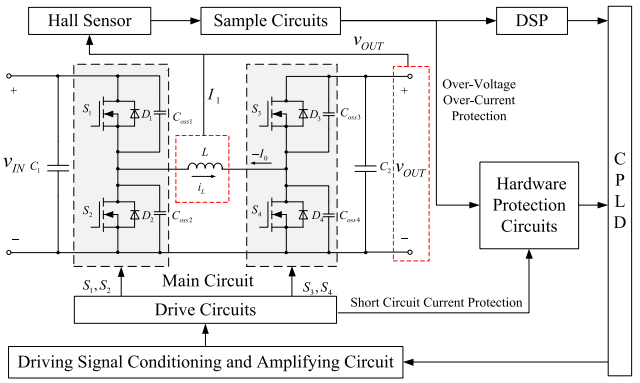


**FIGURE 7.** The overall framework and principle of the experimental CBBC.

The main circuit are constructed according to [21] and [31] with the inductor $L = 13\ \mu H$, input side capacitor and output side capacitor $C_1 = C_2 = 470\ \mu$F. The MOSFET adopts IPW60R099C6. In the sectional control, the inductor is chosen as 1mH. Due to the hardware limitation, the switching frequency is set as 12.8kHz. In the experiment, the variable $D_2$ is set as 0.2 after optimization and $-I_0$ is chosen as $-0.5$A. A large value of $-I_0$ reduces the power transmission efficiency, while a very small value will affect the soft-switching. Based on [32], the range of $-I_0$ should meet following constraint:

$$I_0 \geq \max\left(V_{IN}, V_{OUT}\right)\sqrt{\frac{C_{oss}}{L}} \tag{28}$$

*Remark 3:* Due to the limitation of the experimental conditions, the switching frequency of the experiment is set as 12.8 kHz. The proposed soft-switching control can be applied to higher switching frequency.

### A. EFFECTIVENESS OF CLOSED-LOOP CONTROL

The closed-loop control strategies of CBBC with soft-switching modulation in all operating modes are tested. The output voltage was controlled by PI controller which was design according to $-I_0$-based PWM. After the calculation of (16), the PWM wave was adjusted, and the switches operated in new switching sequence to achieve soft-switching. The time periods in each duty cycle can be determined with (14) and (16), so no zero-crossing detection was used.

With the proposed soft-switching control approach for CBBC, the voltage and current waveforms shown in Figure 9 demonstrated the performance with measured $I_1$, while a measured $I_2$ was taken into the proposed approach in Figure 10 where $i_{L1}$, $v_{IN}$ and $v_{OUT}$ represent the inductor current of proposed soft-switching control, input voltage and output voltage. The CBBC was operating in Buck mode with $V_{IN} = 24$V and $V_{OUT} = 15$ V, of which the voltage waveforms and inductor current waveform represented as $i_{L1}$ were shown in Figure 9(a). The voltage and current waveforms of CBBC operating in Boost mode with $V_{IN} = 24$V, $V_{OUT} = 36$V, were shown in Figure 9(b). While Figure 9(c) showed the voltages and current waveforms of CBBC with

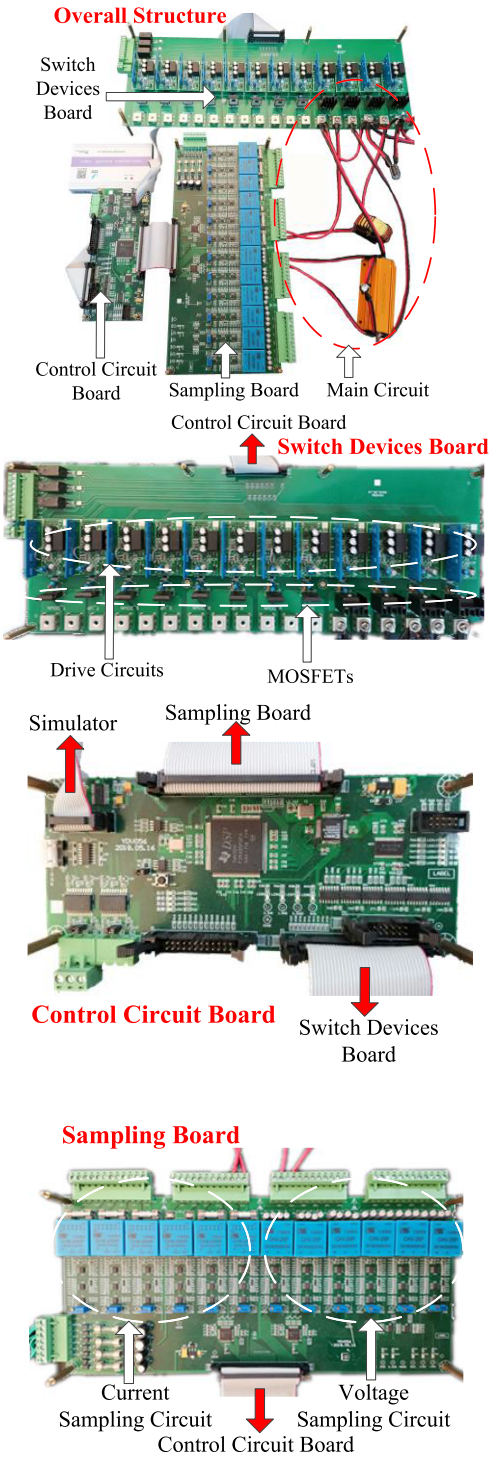


**FIGURE 8.** Experimental 0.2-kW CBBC.

$V_{IN} = V_{OUT} = 24$ V. In addition, the output power was 200W in these experiments. In Figure 9, the ripple current of Buck mode was 39A, Boost mode as 36A and equal-voltage mode was 34A, and $-I_0$ is controlled to be $-2$A. While the ripple current reduced to 37A in Buck mode, 33A in Boost mode and 31A in equal-voltage mode, and $-I_0$ is about $-1$A as shown in Figure10.

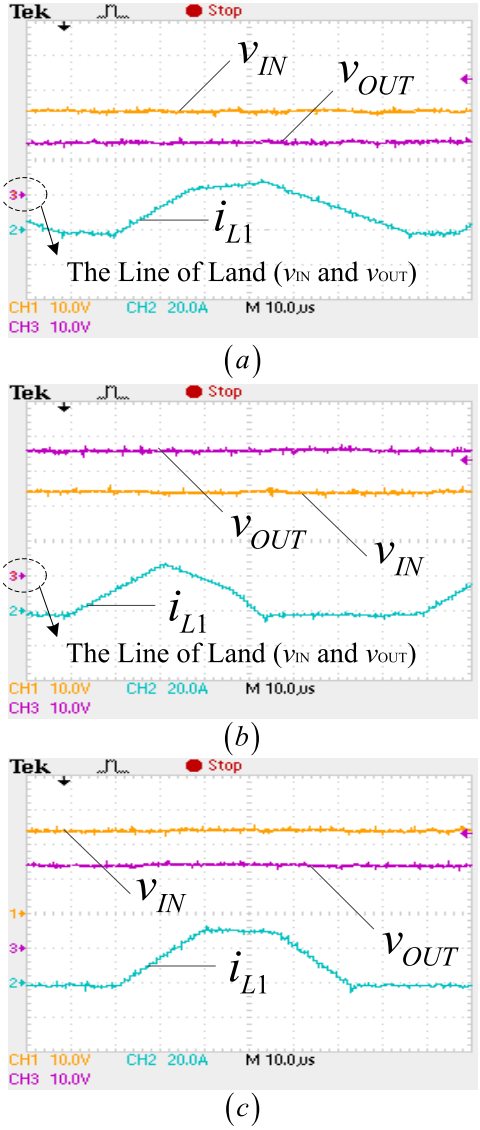


**FIGURE 9.** The voltage and current waveforms of the proposed soft-switching control with measured $I_1$. (a) $V_{OUT} = 15$V and $V_{IN} = 24$V. (b) $V_{OUT} = 36$V and $V_{IN} = 24$V.(c) $V_{OUT} = 24$V and $V_{IN} = 24$V.

The above experimental results showed that CBBC with the proposed control and soft-switching modulation can realize diversiform voltage conversions accurately in Buck, Boost modes and equal-voltage mode. At the same time, the control effect of measuring $I_2$ is better than that of measuring $I_1$, which is mainly reflected in the smaller ripple current and the more accurate calculation of $-I_0$. And the following experiments were based on measured values of $I_2$.

With the developed closed-loop control, the output voltage is kept stable under disturbances. The voltage and current waveforms shown in Figure 11 demonstrated the response to an abrupt load change. The CBBC was operating in Buck mode with $V_{IN} = 24$ V and $V_{OUT} = 36$ V. Two series of tests were carried out in order to obtain a comparison between the load resistance increase and decrease. Both cases used the same control scheme presented in Figure 5. The results of

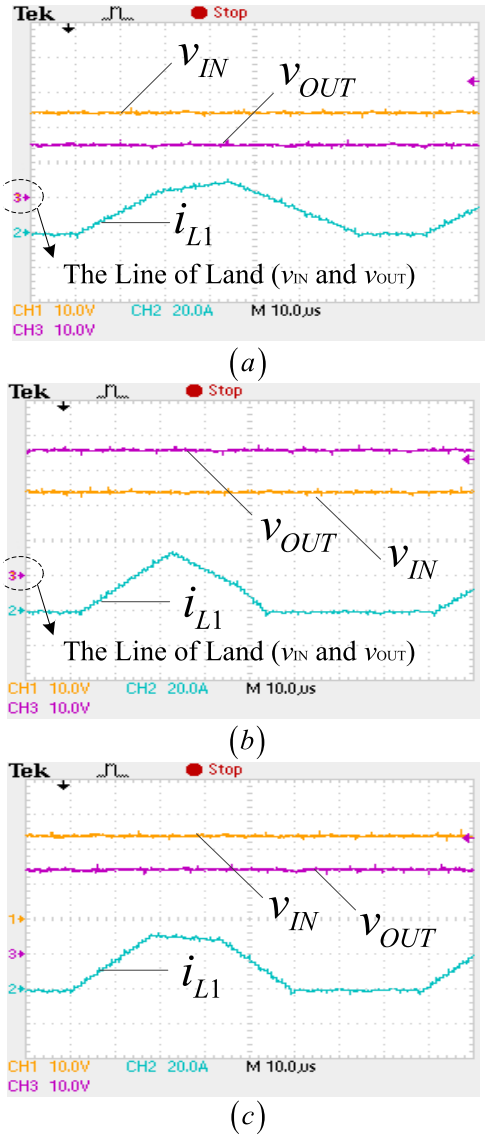


**FIGURE 10.** The voltage and current waveforms of the proposed soft-switching control with measured $I_2$. (a) $V_{OUT}$ = 15V and $V_{IN}$ = 24V. (b) $V_{OUT}$ = 36V and $V_{IN}$ = 24V. (c) $V_{OUT}$ = 24V and $V_{IN}$ = 24V.

the tests under increasing decreasing of the load resistance from 7Ω to 10Ω, was shown in Figure 11(a), and the results of the decreasing load resistance from 10Ω to 7Ω was shown in Figure 11(b), The results indicated the output voltage and inductor current returned to stability after a small oscillation when the load changed. In this way, the tests proved the proposed soft-switching control maintains a safe, reliable, and efficient operation.

### B. VERIFICATION OF SOFT-SWITCHING

To further verify the performance of soft-switching, the waveforms of switches for CBBC with $V_{\rm OUT}$ = 15 V, $V_{\rm IN}$ = 24V were shown in Figure 12, where $v_1$–$v_4$ represented voltages across $S_1$–$S_4$ and $S_1(t)$–$S_4(t)$ were the control signals

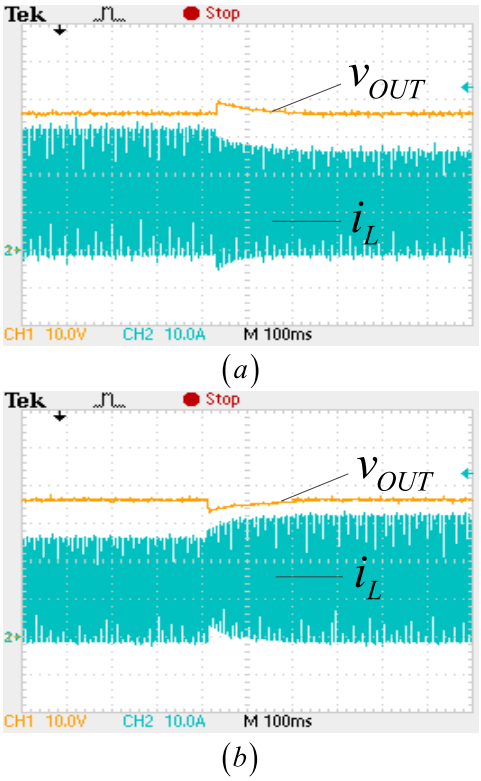


**FIGURE 11.** The voltage and current waveforms of load change test. (a) Increase in the load resistance $R$ = 7 Ω → 10 Ω. (b) Decrease in the load resistance $R$ = 10 Ω → 7 Ω.

of each switch, respectively. Because the currents of the MOSFETs were difficult to measure, inductor current was presented instead. The turn-on and turn-off instants of $S_1$ were showed in Figure 12(a). The soft-switching in turn-on instant of $S_1$ occurred when the control signal $S_1(t)$ increased to driving voltage as 24V while $v_1$ dropped to zero, and the current was zero because it went through the antiparallel body diode $D_1$. The soft-switching in turn-off instant of $S_1$ emerged when $S_1(t)$ reduced to zero before $v_1$ rose from zero to input voltage as 24V, and the current was large than $-I_0$ because it charged the parasitic capacitor $C_{\rm oss1}$ firstly. Similarly, the effects of soft-switching of $S_2$, $S_3$ and $S_4$ were shown in Figure 12(b), (c) and (d). The current went through the antiparallel body diodes to achieve soft-switching when $S_1$–$S_4$ were turned on, and the currents of $S_1$–$S_4$ were zero. When $S_1$–$S_4$ were turned off, the current charged parasitic capacitors first, which makes the currents through $S_1$–$S_4$ close to zero. A lightly delayed turn-on of the $S_1$–$S_4$ in Figure 12(a), (b), (c) and (d) was conducive to fully recharge the parasitic capacitors.

The overall efficiencies for CBBC in all operation modes with the proposed soft-switching control, $-I_0$-based PWM approach and sectional control were measured using a HIOKI 3390 Power Analyzer. The input voltage was 24V and the output voltage was 15V for Buck mode. In Boost mode, the input voltage was set to 24V and the output voltage was set

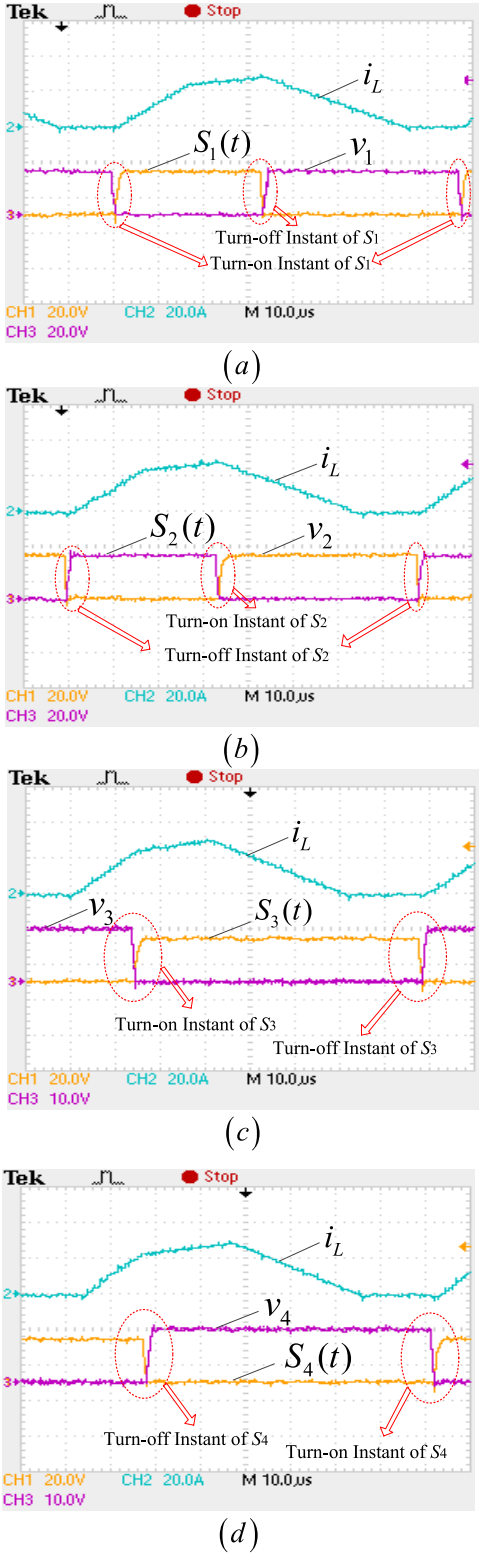


**FIGURE 12.** (a) Soft-switching condition of $S_1$ and $S_2$. (b) Soft-switching condition of $S_3$ and $S_4$.

to 36V. And the input voltage was 24V and the output voltage was 24V for equal-voltage mode. In those tests, the change of output power was achieved by adjusting the output resistor.

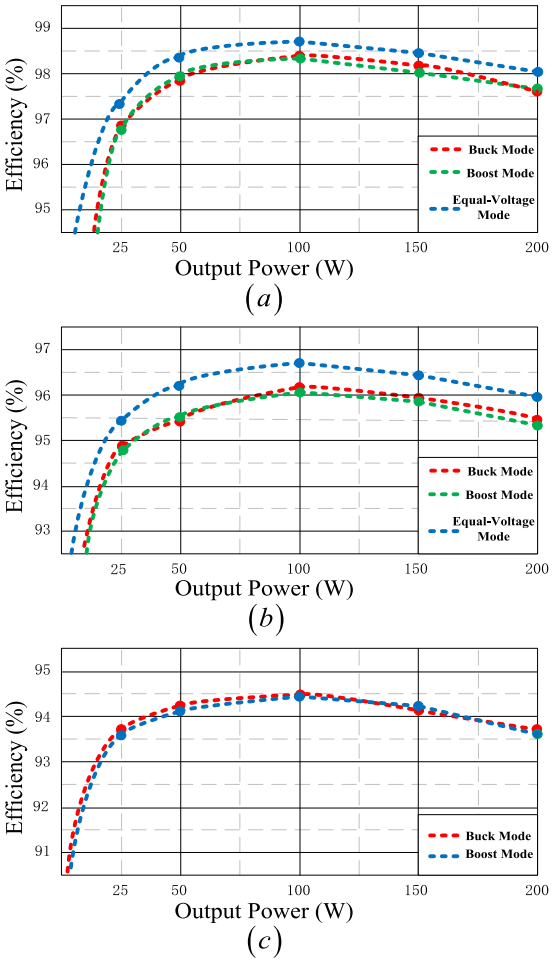


**FIGURE 13.** Measured overall efficiency for CBBC. (a) Proposed soft-switching control. (b)$-I_0$-based PWM control. (c) Sectional control.

**TABLE 2.** Peak efficiency of three modulations.

| Operation Mode | Buck Mode | Boost Mode | Equal-Voltage Mode |
|---|---|---|---|
| Proposed Soft-Switching Control | 98.4% | 98.4% | 98.8% |
| $-I_0$-Based PWM Control | 96.2% | 96.1% | 96.7% |
| Sectional Control | 94.5% | 94.5% | - |

The power conversion efficiency of the three controls were shown in Figure 13(a), (b) and (c), respectively.

It was evident from Figure 13 that with the proposed soft-switching control, a close-to-peak efficiency of about 98.4% of Buck and Boost mode, 98.8% of equal-voltage mode is obtained for the output power ranging from 50W to 200W. Within the same power range, the efficiency of $-I_0$-based PWM control was 96.2% of Buck or Boost mode and 96.5% of equal-voltage mode, and there were approximately 2% lower because of the hard-switching. And the efficiency of sectional control was about 94.5%, owing to the hard-switching and large value of the inductor. And the efficiencies for three approaches were summarized in Table 2. In the

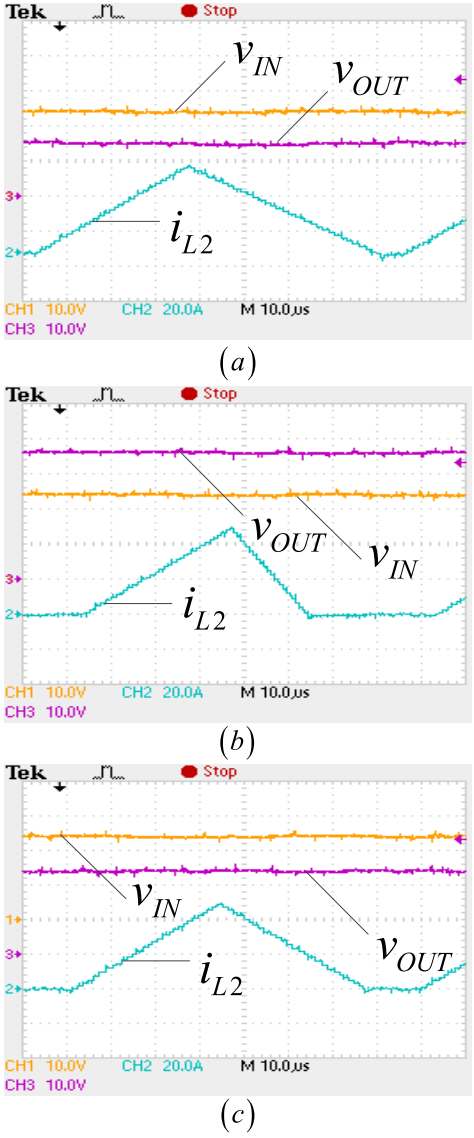


**FIGURE 14.** The current waveforms of $-I_0$-based PWM control. (a) $V_{OUT} = 15V$, $V_{IN} = 24V$. (b) $V_{OUT} = 36V$, $V_{IN} = 24V$. (c) $V_{OUT} = 24V$, $V_{IN} = 24V$.

low-power condition, there was a rapid drop of efficiency due to an increasing loss of inductor at low current [42]. In general, a high efficiency of proposed soft-switching control was maintained over a wide operating range.

### C. VERIFICATION OF RIPPLE CURRENT REDUCTION

The proposed soft-switching control reduces the ripple current by using the optimized duty cycle $D_2$ when comparing to $-I_0$-based PWM control. The inductor current waveforms of CBBC with $-I_0$-based PWM control method in the same operating conditions of Buck, Boost and equal-voltage mode were shown in Figure 14(a), (b) and (c) where $i_{L2}$ represented the inductor current with $-I_0$-based PWM control. While the ripple currents of proposed soft-switching control can be found in Figure 10(a), (b), and (c). As seen from the Figure 14, the ripple current was 47A in Buck mode, 48A in Boost mode and 48A in equal-voltage mode. The comparison of ripple current between soft-switching control and $-I_0$-based PWM control was listed in Table 3. By comparing the two controls, it is clear that the ripple current can be reduced sufficiently by the proposed soft- switching control.

**TABLE 3.** Ripple current of two modulations.

| Operation Mode | Soft-Switching Control | $-I_0$-Based PWM Control |
|---|---|---|
| Buck Mode | 37A | 47A |
| Boost Mode | 33A | 48A |
| Equal-Voltage Mode | 31A | 48A |

## V. CONCLUSIONS

This paper proposed a soft-switching control method for CBBC, and the features of the proposed soft-switching control can be outlined as follows:

1) It is a modification of PWM based on $-I_0$-based PWM modulation and its closed-loop control.

2) By modeling the CBBC with $-I_0$-based PWM and the soft-switching modulation, the relationship between the duty cycles of the two modulations is deduced.

3) No zero-crossing detection of inductor current is required, and $-I_0$ in the proposed method can be controlled as a small value, so the transmission power and the efficiency of CBBC are improved.

4) An optimal design of $D_2$ that is an additional freedom in the proposed control method is presented to achieve lower ripple current and device losses.

## REFERENCES

[1] B. Mangu *et al.*, "Grid-connected PV-wind-battery-based multi-input transformer-coupled bidirectional DC-DC converter for household applications," *IEEE J. Emerg. Sel. Topics Power Electron.*, vol. 4, no. 3, pp. 1086–1095, Sep. 2016.

[2] G. Xu, C. Shang, S. Fan, X. Hu, and H. Cheng, "A hierarchical energy scheduling framework of microgrids with hybrid energy storage systems," *IEEE Access*, vol. 6, pp. 2472–2483, 2017.

[3] K. Muro, T. Nabeshima, T. Sato, K. Nishijima, and S. Yoshida, "H-bridge Buck-Boost converter with dual feedforward control," in *Proc. PEDS*, Nov. 2010, pp. 1002–1007.

[4] L. Piris-Botalla, G. G. Oggier, A. M. Airabella, and G. O. García, "Power losses evaluation of a bidirectional three-port DC–DC converter for hybrid electric system," *Int. J. Elect. Power Energy Syst.*, vol. 58, no. 58, pp. 1–8, Jun. 2014.

[5] B. Moon *et al.*, "A modified topology of two-switch buck-boost converter," *IEEE Access.*, vol. 5, pp. 17772–17780, 2017.

[6] L. Cong, J. Liu, and H. Lee, "A high-efficiency low-profile zero-voltage transition synchronous non-inverting buck-boost converter with auxiliary-component sharing," *IEEE Trans. Circuits Syst. I, Reg. Papers*, vol. 66, no. 1, pp. 438–449, Jan. 2019.

[7] V. F. Pires, D. Foito, and A. Cordeiro, "A DC–DC converter with quadratic gain and bidirectional capability for batteries/supercapacitors," *IEEE Trans. Ind. Appl.*, vol. 54, no. 1, pp. 274–285, Jan./Feb. 2018.

[8] J. Chen, D. Maksimovic, and R. Erickson, "Buck-boost PWM converters having two independently controlled switches," in *Proc. PESC*, Jun. 2001, pp. 736–741.

[9] P.-C. Huang, W.-Q. Wu, H.-H. Ho, and K.-H. Chen, "Hybrid buck–boost feedforward and reduced average inductor current techniques in fast line transient and high-efficiency buck–boost converter," *IEEE Trans. Power Electron.*, vol. 25, no. 3, pp. 719–730, Mar. 2010.

[10] X.-E. Hong, J.-F. Wu, and C.-L. Wei, "98.1%-98.1%-Efficiency hysteretic-current-mode noninverting buck–boost DC-DC converter with smooth mode transition," *IEEE Trans. Power Electron.*, vol. 32, no. 3, pp. 2008–2017, Mar. 2017.

[11] P.-J. Liu and C.-W. Chang, "CCM noninverting buck–boost converter with fast duty-cycle calculation control for line transient improvement," *IEEE Trans. Power Electron.*, vol. 33, no. 6, pp. 5097–5107, Jun. 2018.

[12] P. Liu, C. Chen, S. Duan, L. Jin, and W. Zhu, "A three-level rectifier structure with flying capacitors for DC–DC converter in high-voltage output application," *IEEE Trans. Ind. Electron.*, vol. 65, no. 3, pp. 2122–2134, Mar. 2018.

[13] L.-L. Li, C.-M. Lv, M.-L. Tseng, and M. Song, "Renewable energy utilization method: A novel Insulated Gate Bipolar Transistor switching losses prediction model," *J. Cleaner Prod.*, vol. 176, pp. 852–863, Mar. 2018.

[14] J. Wang and S. Chung, "A novel RCD level shifter for elimination of spurious turn-on in the bridge-leg configuration," *IEEE Trans. Power Electron.*, vol. 30, no. 2, pp. 976–984, Feb. 2014.

[15] T. Konjedic, L. Korošec, M. Truntič, C. Restrepo, M. Rodič, and M. Milanovič, "DCM-based zero-voltage switching control of a bidirectional DC–DC converter with variable switching frequency," *IEEE Trans. Power Electron.*, vol. 31, no. 4, pp. 3273–3288, Apr. 2016.

[16] H.-L. Do, "Improved ZVS DC-DC converter with a high voltage gain and a ripple-free input current," *IEEE Trans. Circuits Syst. I, Reg. Papers*, vol. 59, no. 4, pp. 846–853, Apr. 2012.

[17] I.-O. Lee and G.-W. Moon, "Soft-switching DC/DC converter with a full ZVS range and reduced output filter for high-voltage applications," *IEEE Trans. Power Electron.*, vol. 28, no. 1, pp. 112–122, Jan. 2013.

[18] N. Molavi, E. Adib, and H. Farzanehfard, "Soft-switched non-isolated high step-up DC–DC converter with reduced voltage stress," *IET Power Electron.*, vol. 9, no. 8, pp. 1711–1718, Jun. 2016.

[19] C. Zhang, P. Li, Z. Kan, X. Chai, and X. Guo, "Integrated half-bridge CLLC bidirectional converter for energy storage systems," *IEEE Trans. Ind. Electron.*, vol. 65, no. 5, pp. 3879–3889, May 2018.

[20] Z. M. Dalala, Z. U. Zahid, O. S. Saadeh, and J.-S. Lai, "Modeling and controller design of a bidirectional resonant converter battery charger," *IEEE Access*, vol. 6, pp. 23338–23350, 2018.

[21] C. H. Chien and Y. H. Wang, "ZVS DC/DC converter with series half-bridge legs for high voltage application," *Int. J. Circuit Theory Appl.*, vol. 41, no. 4, pp. 369–386, Apr. 2013.

[22] G. Chen *et al.*, "A family of zero-voltage-switching magnetic coupling nonisolated bidirectional DC–DC converters," *IEEE Trans. Ind. Electron.*, vol. 64, no. 8, pp. 6223–6233, Aug. 2017.

[23] J.-W. Yang and H.-L. Do, "High-efficiency bidirectional DC–DC converter with low circulating current and ZVS characteristic throughout a full range of loads," *IEEE Trans. Ind. Electron.*, vol. 61, no. 7, pp. 3248–3256, Jul. 2014.

[24] R. H. Ashique and Z. Salam, "A high-gain, high-efficiency non-isolated bidirectional DC–DC converter with sustained ZVS operation," *IEEE Trans. Ind. Electron.*, vol. 65, no. 10, pp. 7829–7840, Oct. 2018.

[25] Y. Shen, W. Zhao, Z. Chen, and C. Cai, "Full-bridge LLC resonant converter with series-parallel connected transformers for electric vehicle on-board charger," *IEEE Access*, vol. 6, pp. 13490–13500, 2018.

[26] K.-H. Chao and C.-H. Huang, "Bidirectional DC-DC soft-switching converter for stand-alone photovoltaic power generation systems," *IET Power Electron.*, vol. 7, no. 6, pp. 1557–1565, Jun. 2014.

[27] R. Gurunathan and A. K. S. Bhat, "Zero-voltage switching dc link single-phase pulsewidth-modulated voltage source inverter," *IEEE Trans. Power Electron.*, vol. 22, no. 5, pp. 1610–1618, Sep. 2007.

[28] D.-Y. Jung, S.-H. Hwang, Y.-H. Ji, J.-H. Lee, Y.-C. Jung, and C.-Y. Won, "Soft-switching bidirectional DC/DC converter with a LC series resonant circuit," *IEEE Trans. Power Electron.*, vol. 28, no. 4, pp. 1680–1690, Apr. 2013.

[29] Y. Tsuruta and A. Kawamura, "QRAS and SAZZ chopper for 1EV drive application," in *Proc. PCC*, Nagoya, Japan, Apr. 2007, pp. 1260–1267.

[30] I.-O. Lee and G.-W. Moon, "Half-bridge integrated ZVS full-bridge converter with reduced conduction loss for electric vehicle battery chargers," *IEEE Trans. Ind. Electron.*, vol. 61, no. 8, pp. 3978–3988, Aug. 2014.

[31] J.-B. Baek, W.-I. Choi, and B.-H. Cho, "Digital adaptive frequency modulation for bidirectional DC–DC converter," *IEEE Trans. Ind. Electron.*, vol. 60, no. 11, pp. 5167–5176, Nov. 2013.

[32] S. Waffler and J. W. Kolar, "A novel low-loss modulation strategy for high-power bidirectional buck + boost converters," *IEEE Trans. Power Electron.*, vol. 24, no. 6, pp. 1589–1599, Jun. 2009.

[33] P. Vinciarelli, "Buck-boost DC-DC switching power conversion," U.S. Patent 6 788 033 B2, Sep. 7, 2004.

[34] H. J. Chiu, Y.-K. Lo, S.-W. Kuo, S.-J. Cheng, and F.-T. Lin, "Design and implementation of a high-efficiency bidirectional DC-DC Converter for DC micro-grid system applications," *Int. J. Circuit Theory Appl.*, vol. 42, no. 11, pp. 1139–1153, Nov. 2015.

[35] N. A. Dung, P. P. Hieu, H.-J. Chiu, Y.-C. Hsieh, and J.-Y. Lin, "A DSP based digital control strategy for ZVS bidirectional Buck+Boost converter," in *Proc. 3rd IGBSG*, Apr. 2018, pp. 1–4.

[36] Z. Zhou, H. Li, and X. Wu, "A constant frequency ZVS control system for the four-switch buck-boost DC-DC converter with reduced inductor current," *IEEE Trans. Power Electron.*, to be published.

[37] Z. Yu, H. Kapels, and K. F. Hoffmann, "A novel control concept for high-efficiency power conversion with the bidirectional non-inverting buck-boost converter," in *Proc. EPE ECCE Eur.*, Sep. 2016, pp. 1–10.

[38] Q.-C. Zhong, W.-L. Ming, X. Cao, M. Krstic, "Control of ripple eliminators to improve the power quality of DC systems and reduce the usage of electrolytic capacitors," *IEEE Access*, vol. 4, pp. 2177–2187, 2016.

[39] M. Schormans, V. Valente, and A. Demosthenous, "A low-power, wireless, capacitive sensing frontend based on a self-oscillating inductive link," *IEEE Trans. Circuits Syst. I, Reg. Papers.*, vol. 65, no. 9, pp. 2645–2656, Jul. 2018.

[40] D.-H. Kim and B.-K. Lee, "An enhanced control algorithm for improving the light-load efficiency of noninverting synchronous buck–boost converters," *IEEE Trans. Power Electron.*, vol. 31, no. 5, pp. 3395–3399, May 2016.

[41] Z. Chen, Y. Luo, and M. Chen, "Control and performance of a cascaded shunt active power filter for aircraft electric power system," *IEEE Trans. Ind. Electron.*, vol. 59, no. 9, pp. 3614–3623, Sep. 2012.

[42] *The Datasheet of the Buck Converter Chip Max8646*.

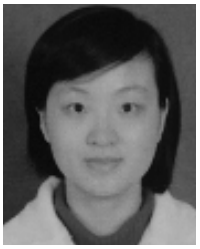

**JINGRONG YU** was born in Dandong, China, in 1981. She received the B.E. and Ph.D. degrees in control science and engineering from Hunan University, Changsha, China, in 2004 and 2009, respectively. From 2014 to 2015, she was a Visiting Scholar with the Department of Electrical Engineering and Computer Science, The University of Tennessee, Knoxville. In 2009, she joined Central South University, where she is currently an Associate Professor.

Her research interests include modeling and control of power electronic converters in renewable energy systems and microgrids, and analysis and control of power quality.

**MAOYUN LIU** was born in Chongqing, China, in 1994. She received the bachelor's degree in control science and engineering from Shandong University, Shandong, China, in 2016. She is currently pursuing the master's degree in electrical engineering with Central South University. Her research interest includes modeling and control of power electronic converters in renewable energy systems and microgrids.

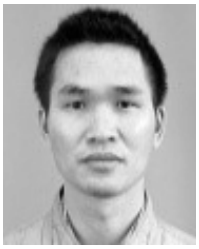

**DONGRAN SONG** received the Ph.D. degree from the School of Information Science and Engineering, Central South University, Changsha, China, in 2016, where he has been an Associate Professor, since 2018. He was a Senior Engineer with China Ming Yang, Zhongshan, from 2009 to 2017, where he took part in designing 1.5–6.0-MW series wind turbines.

**JIAN YANG** (M'09) received the Ph.D. degree in electrical engineering from the University of Central Florida, Orlando, FL, USA, in 2008. He was a Senior Electrical Engineer with Delta Tau Data Systems, Inc., Los Angeles, CA, USA, from 2007 to 2010. Since 2011, he has been with Central South University, Changsha, China, where he is currently an Associate Chair Professor with the School of Automation. His main research interests include control application, motion planning, and power electronics.

**MEI SU** received the B.S., M.S., and Ph.D. degrees from the School of Information Science and Engineering, Central South University, Changsha, China, in 1989, 1992, and 2005, respectively, where she has been a Professor with the School of Automation, since 2006. Her research interests include matrix converter, adjustable speed drives, and wind energy conversion systems.